Finite-precision stationary states at and away from equilibrium

Christoph Dellago

Department of Chemistry, University of Rochester, Rochester, New York 14627-0216

Wm. G. Hoover

Department of Applied Science, University of California at Davis-Livermore, Livermore, California 94551
and Methods Development Group, Department of Mechanical Engineering, Lawrence Livermore National Laboratory,
Livermore, California 94551-7808

We study the precision dependence of equilibrium and nonequilibrium phase-space distribution functions for time-reversible dynamical systems simulated with finite, computational precision. The conservative and dissipative cases show different behavior, with substantially reduced period lengths in the dissipative case. The main effect of finite precision is to change the phase-space fraction occupied by the distributions. The convergence of thermodynamic averages is only slightly affected. We introduce and discuss a simple stochastic model which is nicely consistent with all of our numerical results. This model links the length of periodic orbits to the strange attractor's correlation dimension.

I. INTRODUCTION

''Double precision,'' with approximately 14 decimal digits represented by 48 binary bits, is the usual choice in computation. Thus numerical simulations representing ''continuous'' dynamical systems actually take place on a finite computational grid of states. It is natural to consider and investigate the effect of this finite precision on the ergodicity of flows and on the convergence of time and phase averages as the small-mesh ''continuum limit'' is approached. Such an investigation is timely, because computers are just now becoming fast enough to make such studies possible. Today it is feasible to study billions of iterations of low-dimensional maps and flows, evaluating the influence of finite precision on averages over the numerical evolutions.

Theoretical treatments of chaotic dynamical systems sometimes focus on ''periodic orbits'' [1], trajectories with exact recurrence of an initial phase-space point. It is natural to consider and explore the time-periodic structures from finite-precision simulations by generating such periodic orbits numerically. Evidently any deterministic algorithm must in principle result in a periodic orbit. As the computational precision is increased, the number and lengths of these periodic orbits determine the rate of numerical convergence to the continuum limit. An empirical finding, dating from the early days of computer simulation, is that 14 digits are enough. We consider the details here by studying the effect of reduced precision—from one to 14 decimal digits—for two kinds of representative systems, maps and flows. Both these system types are investigated here at and away from equilibrium. The actual systems considered are detailed in Secs. II and III. Numerical results, followed by a straightforward ''stochastic model'' consistent with them, make up Secs. IV through VI. A discussion section interpreting these results concludes the paper.

II. GALTON BOARD

The Galton board problem [2–8] follows the progress of a mass point with velocity $(\dot{x},\dot{y})=p/m$, driven by an external field E. The moving particle undergoes collisions with a periodic (triangular-lattice) array of hard-disk scatterers. The disk diameter is σ. Consider first the ''equilibrium'' conservative field-free case. Between hard-disk collisions the mass-point motion is a straight line:

$$x_t=x_0+\dot{x}_0t, \quad y_t=y_0+\dot{y}_0t. \tag{1}$$

The nonequilibrium case, with the field on, is more interesting. Energy transfer, from the field to the mass point, makes it necessary to thermostat the motion to obtain a stationary state. Between collisions the thermostated motion, with the ''isothermal constraint'' of fixed kinetic energy (fixed kinetic temperature, with $p^2 \equiv mkT$) follows a transcendental trajectory. The motion equations follow from Gauss's principle of least constraint [1,2,4]:

$$\dot{x}=\frac{p_x}{m}, \ \dot{y}=\frac{p_y}{m}, \ \dot{p}_x=E-\zeta p_x, \ \dot{p}_y=-\zeta p_y, \tag{2}$$

$$\zeta=E\frac{p_x}{p^2}. \tag{3}$$

The friction coefficient ζ is chosen to keep the kinetic energy ($p^2/2m$) constant. Any trajectory resulting from these nonequilibrium motion equations has an analytic solution [6]. But, in practice, it is simpler to generate the trajectories with fourth-order Runge-Kutta integration. The geometry of the Galton board is shown in Fig. 1. Figure 2 shows the distribution of collisions for a (relatively strong) field of $E=4(p^2/m\sigma)$ pointing in a direction parallel to a row of nearest neighbors. We adopt the usual special choice of the scatterer density—$\frac{4}{5}$ the maximum possible density. The motion takes place in a three-dimensional constant-temperature phase space. The two-dimensional distribution shown in the figure is a Poincaré section, with individual points corresponding to collisions, as detailed in Sec. IV. The Poincaré section is multifractal, with a box-counting dimension of
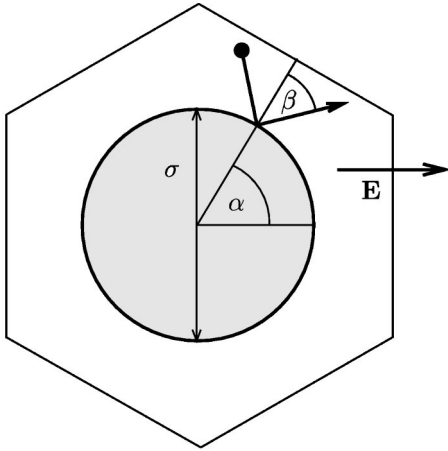
FIG. 1. Unit cell of the periodic Galton board. The field **E** is parallel to a row of nearest neighbors.

$D_{BC} = 2.00$, an information dimension of $D_I = 1.54$, and a correlation dimension of $D_C = 1.43$. See [3] and [10] for definitions of all these fractal dimensions.

III. TIME-REVERSIBLE DISSIPATIVE SHEAR MAP

The second model we consider here is a time-reversible dissipative ergodic map **M**. This dissipative shear map was developed [5] to mimic the time-reversible compressible phase-space flows of nonequilibrium many-body systems. The map **M** maps a point (x, y) in the periodic unit square, centered at the origin with $(-0.5 < x < +0.5)$ and $(-0.5 < y < +0.5)$, onto the ''next'' point (x', y') in the same 1×1 square. The map **M** can be written as a combination of two area-preserving incompressible shear maps **X** and **Y** and a compressible dissipative map **P**:

$$\mathbf{M} = \mathbf{XYPYX}. \tag{4}$$

X and **Y** are shear maps with unit strain (the combination **XY** is the so-called cat map [10]):

$$\mathbf{X}:(x' = x + y; \quad y' = y), \tag{5}$$

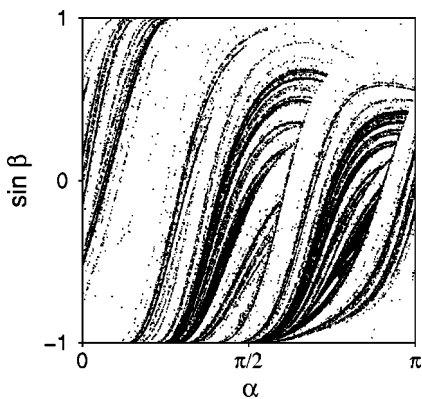$$\mathbf{Y}:(x' = x; \quad y' = x + y). \tag{6}$$

FIG. 2. Distribution of collision points for the periodic Galton board at $E = 4(p^2/m\sigma)$ and $\frac{4}{5}$ of the maximum scatterer density.
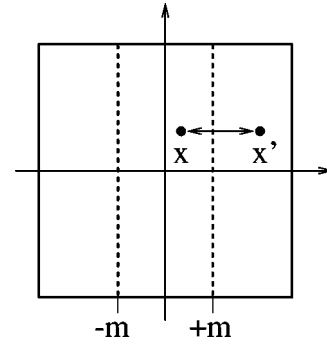

FIG. 3. The map **P** maps the x coordinate of a point (x, y) with $x > 0$ onto its proportional mirror image in a mirror placed at m. Similar operations are carried out for negative x, as shown in the figure, and for the y coordinate.

Periodic boundary conditions ensure that the images generated by **X** and **Y**, and indicated above by primes, lie in the unit square. The map **P**, for ''proportional,'' corresponds to a reflection of both the x and y coordinates in ''mirrors'' placed at the locations $\pm m$ on both the x and y axes. The reflection operation is illustrated in Fig. 3 for reflection of the positive x coordinate. Such a coordinate is mapped onto the next coordinate x':

$$x' = m + (m - x)\left(\frac{1 - 2m}{2m}\right) \quad \text{if} \quad x < m \tag{7}$$

and

$$x' = m - (x - m)\left(\frac{2m}{1 - 2m}\right) \quad \text{if} \quad x > m. \tag{8}$$

Analogous operations are carried out for negative x coordinates and for y coordinates. For the special value $m = \frac{1}{4}$ the map **P** is incompressible and preserves area exactly, $dx'dy' = dxdy$. For all other choices of m there are coexisting expanding and contracting regions. As a result, the combined map **M** = **XYPYX** produces a multifractal phase-space probability distribution with an information dimension strictly less than 2.

Both the shears and the reflections are time-reversible operations. This means that the ''time-reversed'' point $(x', -y')$ maps into the reversed initial point $(x, -y)$, so that the y coordinate plays the role of a momentum. Because the composite map **M** is simultaneously ergodic, mixing, and time reversible it has all the properties of typical nonequilibrium systems except for the ''flow property'' of obeying a set of ordinary differential equations. Point distributions $\{x, y\}$ generated with the map **M** for different values of $\Delta m \equiv \frac{1}{4} - m$ are shown in Fig. 4.

IV. FINITE-PRECISION DISTRIBUTIONS FOR THE GALTON BOARD

In the Galton board, collisions of the moving particle with the scatterers can be described with two angles α and β. As shown in Fig. 1, the angle α specifies the point where the particle hits the scatterer and β is the angle the outgoing velocity makes with the normal at the collision point. The phase-space flow generated by the equations of motion [6]
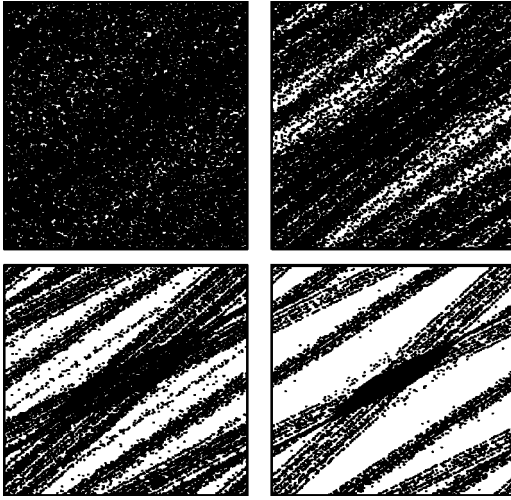
FIG. 4. Point distributions generated with the shear map **M** for $\Delta m \equiv \frac{1}{4} - m = 0.01$ (upper left), $\Delta m = 0.05$ (upper right), $\Delta m = 0.10$ (lower left), and $\Delta m = 0.15$ (lower right).

maps a collision point $(\alpha, \sin \beta)$ forward to a new one $(\alpha', \sin \beta')$. We artificially reduced the precision of the computation by dividing the $(\alpha, \sin \beta)$ plane into $N = n \times n$ equal rectangular cells. Trajectories were generated by randomly selecting one of the cells and taking that cell's center as the initial point $(\alpha, \sin \beta)$. Then, $(\alpha, \sin \beta)$ is mapped to a new collision point $(\alpha', \sin \beta')$, defining the cell from which the next center point is selected for further mapping. This procedure is schematically illustrated in Fig. 5. In an $n \times n$ array of N cells each choice of an initial point eventually results in a subsequent periodic orbit of length less than or equal to $N = n^2$.

The sampling of all possible trajectories can be made exhaustive for n less than a few thousand. These coarse-mesh results establish the presence of occasional ''fixed points'' (center points that map into the same cell) together with a relatively large attractive periodic orbit. In some cases there are additional smaller periodic orbits too, but generally a
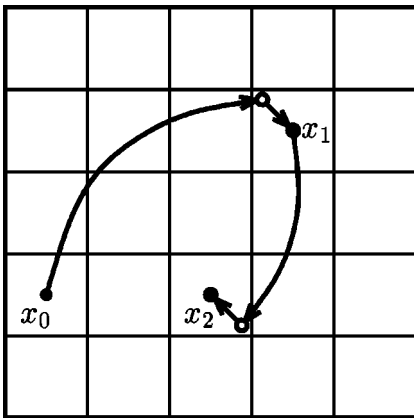

FIG. 5. To artificially reduce the precision of the computation we partition phase space into N equal cells and identify all points in a cell with the cell's center. Starting from a point x_0 the mapping is carried out with full precision, producing the point x_1' (open circle), which is then mapped onto the center x_1 of its box (full circle). Iteration of this procedure yields deterministic finite-precision trajectories.
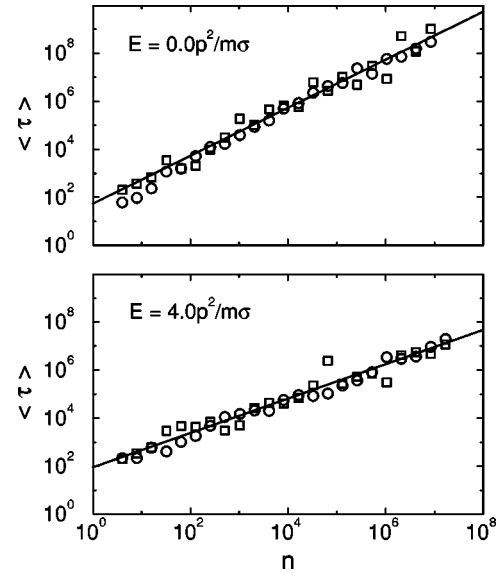

FIG. 6. Average transient length (circles) and average period length (squares) for the periodic Galton board for $E = 0.0p^2/m\sigma$ (top) and $E = 4.0p^2/m\sigma$ (bottom) as a function of the number n of cells per side. The two-dimensional $(\alpha, \sin \beta)$ collision space is divided into a total of $N = n^2$ cells. The average total length of a trajectory is the sum of the average transient and the average period. The straight lines have slopes $D_C/2 = 1.000$ (top panel) and $D_C/2 = 0.715$ (lower panel).

unique largest periodic orbit is obtained from most of the n^2 initial points. This largest orbit contains only a small fraction of the total cells. Table 1 lists the number of filled cells eventually obtained in the stationary state resulting from the repeated iteration of the smaller maps for both the conservative (field-free) and dissipative versions of the Galton board. These results were obtained with exhaustive sampling and suggest that a negligible fraction of the cells is occupied in the steady state, with that fraction strongly dependent on the extent of dissipation associated with the area change.

Considerably larger grids, with n up to a few million ($N = n^2 \simeq 10^{14}$), can be investigated effectively by choosing for iteration an ensemble of several initial points at random. For each initial point the map is iterated until the trajectory eventually hits a cell that has been visited earlier. For each trajectory we determine the ''length'' (number of collisions) of the transient τ_t before the system reaches the periodic orbit as well as the length of the period τ_p. Figure 6 shows average transient and orbit lengths as a function of the number n of cells per side. The same lengths are listed in Table I. In each simulation we tested at least 1000 initial conditions selected uniformly from the collision space $(\alpha, \sin \beta)$. In the equilibrium case, with $E = 0.0p^2/m\sigma$, both the period and the transient lengths scale roughly linearly with $n = N^{1/2}$, but large deviations from this scaling law can be observed. We studied finite-precision orbits also in the stadium billiard [9] and found the same scaling law. Far from equilibrium, at $E = 4.0p^2/m\sigma$, the transient and period lengths are again roughly equal but scale approximately with $n^{0.7}$. Both at equilibrium and far from equilibrium we typically found fewer than ten different periodic orbits. From one to four orbits attract most of the initial conditions.

These results indicate that trajectories in dissipative sys-

TABLE I. Average transient lengths and average period lengths for the Galton board at $E=0.0p^2/m\sigma$ and $E=4.0p^2/m\sigma$. Each number is an average over at least 1000 initial conditions. The last two columns contain the number of cells occupied in the stationary state for $E=0.0p^2/m\sigma$ and $E=4.0p^2/m\sigma$.

n	$\tau_t(0)$	$\tau_p(0)$	$\tau_t(4)$	$\tau_p(4)$	$N(0)$	$N(4)$
2	0.0	2.0	0.0	2.0	4	4
4	0.6	2.0	2.1	2.0	8	4
8	1.0	3.8	2.2	3.3	32	16
16	2.3	6.7	5.9	5.9	80	16
32	11.7	34.4	4.2	29.3	96	96
64	15.6	15.9	10.3	46.0	276	94
128	52.6	20.5	18.1	44.1	320	116
256	126.3	97.2	48.0	69.9	388	102
512	168.8	311.5	111.2	30.7	1836	216
1024	394.6	1915.4	150.9	50.3	7032	338
2048	851.5	1015.0	203.0	257.3	5240	1046
4096	1591.5	4606.3	201.9	437.2	9152	1682
8192	5004.8	6699.0	577.6	399.6	30092	1836
16384	8277.5	5828.9	905.3	684.0		
32768	22692.7	60374.1	839.7	2297.3		
65536	43449.4	27850.8	1040.6	23966.2		
131072	57687.3	104454.0	2239.1	2713.3		
262144	232650.0	47829.4	3706.3	5403.8		
524288	140072.0	300310.0	8101.3	7239.4		
1048576	578914.0	85361.7	34237.1	3141.5		
2097152	715255.0	5127410.0	29527.9	41280.3		
4194304	1560570.0	1157840.0	36654.0	55457.1		
8388608	2996410.0	10137800.0	93331.7	47429.2		

tems in which the phase-space density collapses onto a multifractal attractor are shorter than trajectories in conservative systems. More specifically, the exponent γ describing the scaling of period lengths, $\tau_p \simeq n^\gamma$, decreases with increasing departure from equilibrium.

V. FINITE-PRECISION DISTRIBUTIONS FOR THE SHEAR MAP

The results presented in the previous section suggest that there exists a relation between the scaling of periodic orbit lengths and the multifractal properties of the system. To study this relation more systematically we carried out a more detailed finite-precision analysis on the dissipative shear map [5]. This map is computationally less complex than the Galton board and thus allows a more thorough investigation. Period lengths up to more than one billion can be investigated. Figure 7 shows the length τ_p of the longest periodic orbits as a function of the number n of cells per side for three different mirror positions: $\{\Delta m\}=\{0.00, 0.08, 0.16\}$. The finest grid for $\Delta m=0.16$ contains $N \simeq 8 \times 10^{28}$ cells. For $\Delta m=0.00$ the map is conservative, with all its fractal dimensions equal to the full phase-space dimension of $D=2$. The dynamics is dissipative, with overall contraction, for $\Delta m=0.08$ and $\Delta m=0.16$, leading to information and correlation dimensions substantially smaller than the full phase-space dimension. Just as in the case of the Galton board an increase in the applied nonequilibrium perturbation lowers these frac-
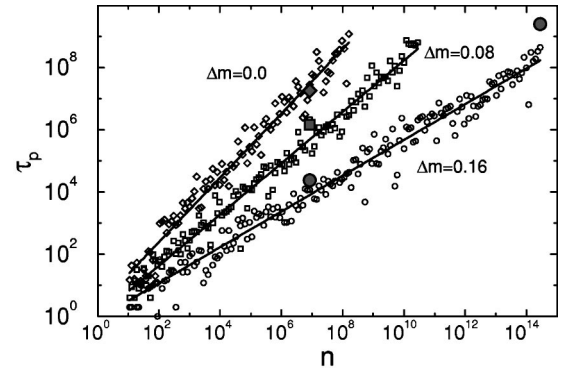

FIG. 7. Length of the longest periodic orbit for the shear map **M** as a function of the number n of cells per side for $\Delta m=0.00$ (circles), $\Delta m=0.08$ (squares), and $\Delta m=0.16$ (diamonds). Lines are linear fits to the simulation results. The larger gray symbols denote periodic orbits found without artificially reducing the precision with single precision arithmetic (23 bits) and double precision arithmetic (48 bits)

tal dimensions. The results shown in Fig. 7 indicate that the maximum period length is approximately equal to $\tau_p \simeq n^\gamma$, where the scaling exponent γ decreases with increasing dissipation.

The period lengths we found for the shear map **M** and presented in Fig. 7 suggested that it should be possible to find periodic orbits even without any artificial reduction of the precision. This is true. We have observed such periodic orbits for both single precision, 23 bits, corresponding to 8.3×10^6 cells per side, and double precision, 48 bits, corresponding to 2.8×10^{14} cells per side. In Fig. 7 the lengths of these orbits are indicated by large gray symbols. The periodic orbits with conventional single and double precision have lengths following exactly the same scaling relation as the periodic orbits generated with artificially reduced precision. This observation indicates that our method of reducing the precision faithfully represents the truncation of floating point numbers that occurs naturally in computer programs.

To study the dependence of the scaling exponent γ on the parameter Δm we have fitted straight lines to plots of $\ln \tau_p$ versus $\ln n$ for different values of Δm. The corresponding scaling exponents γ are obtained from the slopes of these lines. Figure 8 shows the scaling exponent γ along with $D_C/2$ as a function of Δm. The correlation dimension D_C has been determined by box counting using double precision arithmetic [10]. Clearly, the relation $\gamma=D_C/2$ holds over the
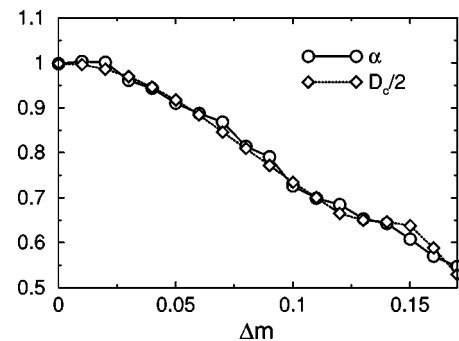

FIG. 8. Scaling exponent γ and half the correlation dimension $D_C/2$ for the shear map **M** as a function of the parameter Δm.

whole range of Δm. Thus, *the correlation dimension of the underlying attractor is very simply related to the length of typical periodic orbits caused by the finite precision of the computation.* We show how this comes about in the following section.

VI. STOCHASTIC MODEL

The main result of the two preceding sections is that finite-precision arithmetic leads to periodic orbits with length $\tau_p \simeq n^\gamma$, where the scaling exponent γ is unity at equilibrium and varies with $D_C/2$ as the system is driven away from equilibrium. Typically, the transient that occurs before the system settles into a periodic orbit has about the same length as does the periodic orbit. Furthermore, most initial conditions converge to a small number of periodic orbits. All these results can be rationalized with a simple stochastic model, as explained below.

We recently came across earlier relevant work of Grebogi, Ott, and Yorke [12] and Lanford [13]. Grebogi, Ott, and Yorke's article contains most of the results obtained here for the stochastic model described in this section. Despite this duplication, we believe that the results given here, in our own paper, are significant and interesting in their own right. In particular, the old ideas turn out to be nicely consistent with the much more detailed and realistic statistical-mechanical models we could study using present-day computing machines.

As a very crude caricature of the systems we have studied so far, consider a system that can reside in any of N cells. We imagine a dynamics for this system such that at each discrete time the system jumps randomly to one of the N cells. For simplicity, we first consider the case of uniform probability. In this case the probability of jumping into cell i is always $p_i = 1/N$. Imagine now that this ''stochastic'' system starts in a certain cell and performs random jumps until it again hits a cell visited earlier. At the moment this occurs that cell, and that cell alone, has been visited twice, and for the first time. Because we want to use this stochastic model to understand deterministic dynamics we assume that once the system revisits any cell it is subsequently trapped in a periodic orbit of length τ_p. Thus, the total number of cells visited, starting from a certain initial condition, is $\tau_c = \tau_p + \tau_t$, where τ_t is the length of the transient before the system first visits a cell belonging to the periodic orbit. This mechanism is indicated schematically in Fig. 9.

We can calculate the probability $P(\tau_c, N)$ of a trajectory with total length τ_c in a system of N cells by requiring that the trajectory does not recross itself during the first $\tau_c - 1$ steps, but hits a cell that has already been visited on step τ_c:

$$P(\tau_c, N) = \prod_{i=1}^{\tau_c - 1} \left(1 - \frac{i}{N}\right) \frac{\tau_c}{N} = \frac{\tau_c}{N^{\tau_c}} \frac{(N-1)!}{(N-\tau_c)!}. \quad (9)$$

This problem is akin to the ''birthday problem,'' discussed, for instance, in [11], which consists of calculating the probability that at least two of a group of people have the same birthday. For large N relation (8) can be used to derive a differential equation for $P(\tau_c, N)$ whose solution is
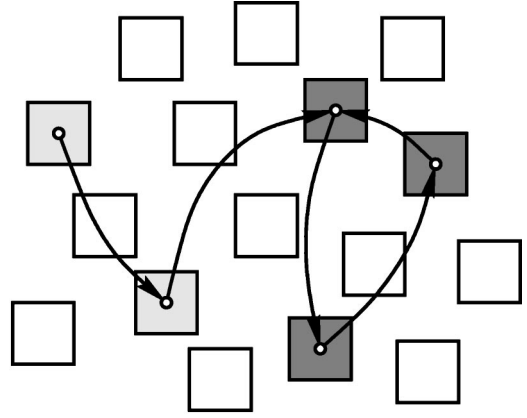

FIG. 9. In the stochastic model we imagine that the system performs random jumps between N cells. Once one of the cells is revisited, the system settles onto a periodic orbit. The trajectory shown in the figure starting in the upper left corner has a transient length of 2, a period length of 3, and a total length of 5.

$$P(\tau_c, N) = \frac{\tau_c}{N} \exp\left(-\frac{\tau_c^2}{2N}\right). \quad (10)$$

The average and the variance of the trajectory lengths are as follows:

$$\langle \tau_c \rangle = \sqrt{\frac{\pi N}{2}}, \quad (11)$$

$$\sqrt{\langle (\tau_c - \langle \tau_c \rangle)^2 \rangle} = \sqrt{N\left(2 - \frac{\pi}{2}\right)}. \quad (12)$$

Next, we calculate the distribution of transient and period lengths. A trajectory of total length τ_c can contribute to all period lengths from 1 to τ_c. Because all intersection points have equal probabilities we can obtain the distribution of large-N period lengths τ_p by integration over all total trajectory lengths from τ_p to N (or to infinity for very large N):

$$P(\tau_p, N) = \int_{\tau_p}^{\infty} d\tau_c \frac{P(\tau_c, N)}{\tau_c} = \sqrt{\frac{\pi}{2N}} \text{erfc}\left(\frac{\tau_p}{\sqrt{2N}}\right). \quad (13)$$

The average and the variance of the period length are

$$\langle \tau_p \rangle = \sqrt{\frac{\pi N}{8}}, \quad (14)$$

$$\sqrt{\langle (\tau_p - \langle \tau_p \rangle)^2 \rangle} = \sqrt{N\left(\frac{2}{3} - \frac{\pi}{8}\right)}. \quad (15)$$

The distribution of transients is identical to the distribution of periods in the stochastic model. Thus, the stochastic model succeeds in reproducing the square root scaling laws for period and transient lengths found numerically for the Galton board and the shear map **M** in equilibrium. This suggests that scaling with $\sqrt{N}$ is a consequence of the statistics of the mapping and that the details of the dynamics are of minor importance for the scaling.

The stochastic model can also be used to understand the fact that most initial conditions converge onto a small number of periodic orbits. Imagine having generated a trajectory with total length of approximately $\sqrt{N}$ in the stochastic

model. Now calculate the probability of generating another trajectory of length $\sqrt{N}$ differing from the first one *at every point* (for otherwise they would lead to the same periodic orbit). This probability is obtained by multiplying the probability of missing all the cells belonging to the first trajectory at all $\sqrt{N}$ steps of the second trajectory:

$$P_{\mathrm{miss}} = \left(1 - \frac{\sqrt{N}}{N}\right)^{\sqrt{N}} \simeq \frac{1}{e}. \tag{16}$$

Similarly, the probability of generating a third trajectory of length $\sqrt{N}$ different from the two previous ones at all points is $1/e^2$. Thus, the probability of finding more than a few completely different trajectories of length $\sqrt{N}$ decreases exponentially fast.

The stochastic model described so far is based on the assumption that each cell has the same probability of being visited at each time step: $p_i = 1/N$ for all i. This assumption is justified for ergodic systems in equilibrium at constant energy, in which the available phase space is covered uniformly. Far from equilibrium, however, phase-space distributions have a multifractal structure. To take such highly non-uniform distributions into account we generalize the stochastic model to include the case where the probability p_i of visiting a certain cell i can vary from cell to cell.

With a nonuniform distribution of probabilities periodic orbits and transients become shorter because recurrence becomes more likely in the cells with a large p_i. We have found numerically that in the stochastic model the distributions of total trajectory lengths and period lengths are

$$P(\tau_c, N) = \tau_c S \exp\left(-\frac{\tau_c^2 S}{2}\right) \tag{17}$$

and

$$P(\tau_p, N) = \sqrt{\frac{\pi S}{2}} \mathrm{erfc}\left(\tau_p \sqrt{\frac{S}{2}}\right), \tag{18}$$

where $S \equiv \Sigma_i p_i^2$. The distribution of transient lengths is again identical to the distribution of period lengths. Thus, the distributions for the nonuniform model can be obtained from the distributions for the uniform model simply by replacing the number of cells N with $1/S$.

According to the distributions (17) and (18) average period, transient, and trajectory lengths scale with

$$\langle \tau \rangle \propto S^{-1/2}. \tag{19}$$

To obtain a scaling law for τ as a function of the precision, or, equivalently, as a function of the total number of cells N, we have to consider how S itself scales with the precision. From dynamical systems theory we know that for small cell sizes S the probability of finding two points in the same phase-space cell scales as a power of the cell size, $S \propto \epsilon^{D_C}$, where ϵ is the cell size and D_C is the correlation dimension of the underlying attractor [3,10]. Expressing the cell size ϵ as a function of the number of cells N and the dimensionality D of phase space, $\epsilon \propto N^{-1/D}$, we finally obtain

$$\langle \tau \rangle \propto N^{D_C/2D}. \tag{20}$$

In equilibrium $D_C = D$ and the period length scales with $\sqrt{N}$. Far from equilibrium it is the correlation dimension D_C that determines the lengths of both the transients and the periodic orbits. Thus, the stochastic model reproduces the scaling laws found both at equilibrium and far from it.

VII. DISCUSSION AND CONCLUSIONS

The results of our study show that computational representations of conservative and dissipative systems are different. Conservative maps or dynamical systems exhibit a long ($\simeq \sqrt{N}$) transient period ending in a periodic orbit of about the same length ($\simeq \sqrt{N}$). This behavior closely resembles the quantum ''pseudochaos'' described by Chirikov [14]. Quantum chaotic systems mimic classical behavior up to a ''break time'' at which they are confined to discrete quantum states, whose classical analog is a periodic orbit. Thus the conservative systems we have studied show a long chaotic transient with a length increasing as the square root of the number of phase-space states.

Dissipative systems, on the other hand, have trajectories with transients and orbits of length $\simeq N^{D_C/2D}$. Thus, the dissipative systems show a large basin of attraction with $\simeq N$ states that leads very rapidly to a single periodic orbit. This orbit is the analog of the Sinai-Ruelle-Bowen states [1] and ergodic time-reversible strange attractors [2,3] which caricature and characterize nonequilibrium systems.

Our primary theoretical advance has been to relate the length of periodic orbits to the correlation dimension of the underlying distribution function. Further, deterministic systems evolving on a finite grid of states caused by finite computer precision cannot be ergodic. In fact, for a typical trajectory the fraction of covered cells in phase space is of the order of $N^{-(1-D_C/2D)}$. Our research raises some interesting questions as corollaries. Is it really worthwhile to consider a formal periodic-orbit theory of distributions when the computational work suggests strongly that these orbits have no operational meaning? Chaotic systems can be characterized only by computation. Thus, a theory based on these findings, rather than hypothetical continuous periodic orbits, is desirable. Conservative systems have their own puzzling properties. The gradual increase of the transient evolution, as mesh size decreases or as the number of degrees of freedom increases, guarantees that the small-mesh limiting orbit is (only) a transient. On the other hand, any computer simulation, even one running on a large machine for the age of the universe, is limited to the exploration of relatively short ''transients.''

[1] P. Gaspard, *Chaos, Scattering, and Statistical Mechanics* (Cambridge University Press, Cambridge, England, 1998).

[2] Wm. G. Hoover, *Computational Statistical Mechanics* (Elsevier, Amsterdam, 1991).

[3] Wm. G. Hoover, *Time Reversibility, Computer Simulation, and Chaos* (World Scientific, Singapore, 1999).

[4] J. R. Dorfman, *An Introduction to Chaos in Nonequilibrium Statistical Mechanics* (Cambridge University Press, Cambridge England, 1999).

[5] W.G. Hoover, O. Kum, and H.A. Posch, Phys. Rev. E **53**, 2123 (1996).

[6] B. Moran, W.G. Hoover, and S. Bestiale, J. Stat. Phys. **48**, 709 (1987).

[7] C. Dellago, Ph.D. thesis, University of Vienna, 1995 (unpublished).

[8] J. Petravic, D.J. Isbister, and G.P. Morriss, J. Stat. Phys. **76**, 1045 (1994).

[9] G. Schuster, *Deterministic Chaos: An Introduction* (VCH Verlagsgesellschaft, Weinheim, 1989).

[10] Ya.G. Sinai, Russ. Math. Surv. **25**, 137 (1970).

[11] W. Feller, *An Introduction to Probability Theory and Its Applications* (Wiley, New York, 1968).

[12] C. Grebogi, E. Ott, and J.A. Yorke, Phys. Rev. A **38**, 3688 (1988).

[13] Oscar E. Lanford III, Exp. Math. **7**, 317 (1998).

[14] B. Chirikov, in *Nonlinear Dynamics, Chaotic and Complex Systems*, edited by E. Infeld, R. Żelazny, and A. Galkowski (Cambridge University Press, Cambridge, England, 1997), pp. 149–171.